Experimental Investigation on Thermal Buckling Behavior of Truss-Core Sandwich Panels

Wu Yuan,* Hongwei Song,† Xi Wang,‡ and Chenguang Huang§
Institute of Mechanics, Chinese Academy of Sciences, 100190 Beijing, People's Republic of China

This paper presents an experimental study on the thermal buckling behavior of sandwich panels with truss cores. The ultimate goal is to find the critical buckling temperature and examine postbuckling behavior of this newly developed sandwich panel experimentally. A specifically designed fixture, which can introduce in-plane loads to the sandwich panel through thermal expansion mismatch between the specimen and the load frame, is applied in the experiment. High-temperature strain gauges are attached at the center of the sandwich panel face sheets to measure the local in-plane response, and the critical buckling temperature of panels deformed in symmetric mode is determined by using the Southwell method. To obtain the full-field postbuckling mode as well as critical buckling temperature of the sandwich panel deformed in asymmetric mode in high-temperature environments, a noncontact measurement system based on the three-dimensional digital image correlation technique is also developed. The accuracy of the present noncontact measurement technique is validated by the coordinate measurement machine technique, a conventional contact measurement method. It is found that the critical buckling temperature obtained from experiments is lower than that predicted by theoretical and numerical models, due to defects and imperfections of the truss core and sandwich panel during fabrication. Full-field measurement also indicates that local yielding together with overall buckling is the typical deformation mode in the tested specimen.

Nomenclature

A_{mn}, B_{mn}, C_{mn}	=	Fourier constant coefficients
C, C_s	=	shear stiffness of the sandwich panel
D	=	flexural rigidity of sandwich panels
E	=	modulus of the material
E_s	=	Young's modulus of parent material
E^*	=	Young's modulus of cellular material
F	=	shear force
G_c	=	equivalent shear modulus of the lattice truss core
h_c	=	core thickness
h_p	=	sandwich panel thickness
h_{sn}, h_{rm}	=	coefficients in double Fourier expansion
I_0, I	=	gray value of points on source image and target image
$\bar{I}_0, \bar{I}$	=	average gray value of points on source image and target image
M_x, M_y	=	bending moments
M_{xy}	=	torsional moment
m	=	number of expansion
N, N_x, N_y, N_{xy}, N_T	=	compressive in-plane force
n	=	number of expansion
P	=	pressure load on a column
P_{cr}	=	critical buckling load of the column
Q_x, Q_y	=	shear force
S	=	cross-section area of truss cores
t	=	thin-plate thickness
u, v, w	=	displacements
$[u]$	=	matrix of Fourier constant coefficients
w_0	=	displacement at the middle-plane
α	=	coefficient of thermal expansion of the sandwich panel
α_m, β_n	=	coefficients in double Fourier expansion
γ_r, ψ_s	=	coefficients in double Fourier expansion
Δ_{pyramid}	=	displacement of unit cell of truss cores
ΔT_{cr}	=	critical buckling temperature
ΔT	=	temperature rise
δ	=	lateral deflection of the midpoint of the column
δ_0	=	initial deflection of the imperfect column
ε_b	=	bending strain in the center of the sandwich panel
$\varepsilon_{\text{pyramid}}$	=	shearing strain of truss cores
η	=	correction factor
μ	=	Poisson's ratio
$\bar{\rho}$	=	relative density of truss core
ϕ_x, ϕ_y	=	rotations of the normal in the x-z and y-z planes
ω	=	angle between the truss and the panel

*Ph.D. Student, Key Laboratory for Mechanics in Fluid Solid Coupling Systems, No. 15 Beisihuanxi Road.

†Professor, Key Laboratory for Mechanics in Fluid Solid Coupling Systems, No. 15 Beisihuanxi Road; songhw@imech.ac.cn (Corresponding Author).

‡Associate Professor, Key Laboratory for Mechanics in Fluid Solid Coupling Systems, No. 15 Beisihuanxi Road; xiwang@imech.ac.cn.

§Professor, Key Laboratory for Mechanics in Fluid Solid Coupling Systems, No. 15 Beisihuanxi Road; huangcg@imech.ac.cn.

I. Introduction

THERMAL buckling is probably the most important effect of high temperatures in thin-walled structures, besides the degradation of material properties [1]. When being used as load bearing components in a thermal protection system of high-speed flight, the sandwich panel may buckle due to the in-plane load caused by the thermal inhomogeneity. Therefore, to integrate a sandwich panel with a truss core, a novel lightweight multifunctional structure, into a flight-ready aircraft, the response of the panel to in-plane thermomechanical loading becomes a driving design parameter. However, as Rakow and Waas [2,3] commented, previous investigations into sandwich panels under thermal loading are almost exclusively numerical and theoretical in nature; very few efforts have analyzed the thermomechanical response of sandwich panels experimentally.

There have been some experimental studies on the thermal buckling behavior of thin plates and laminates [4–6]. A benchmark

thermal buckling test of a thin plate subjected to a nonuniform temperature environment was carried out by Gossard et al. [4]. In their work, a thermal load was applied by using electric heaters that were in the center of the plate, yielding the tentlike temperature distribution. The boundary conditions were simply supported at two sides of the plate, and the others were uniform heat sinks supplied by cooling water. Deflections of the plate were measured by dial gauges. Murphy and Ferreira [5] carried out the thermal buckling experiment of a fully clamped, rectangular plate subjected to uniform thermal environment. However, because of the effect of heat conduction of the boundary constraint, the edge temperature was typically 90% of the center temperature. For thermal buckling experiments, the importance of appropriate boundary conditions even exceeds other factors in usual buckling experiments [1]. Blosser [7] pointed out some of the problematic characteristics and interactions between thermal and structural boundary conditions. Richards and Thompson [8] carried out thermal buckling experiments for the titanium honeycomb sandwich panels. In their experiment, there was a conflict between the thermal and structural boundary conditions; the thermal boundary conditions are corrupted by the presence of mechanical boundary conditions, acting as a heat sink. To address this problem, Rakow and Waas [2] developed a novel experimental technique. The central concept was introducing in-plane loads to the specimen by mismatched coefficients of thermal expansion (CTEs) between the specimen and the fixture. The critical buckling temperature (CBT) and postbuckling behavior of the foam sandwich panels were measured by strain gauges and shadow moiré interferometry.

Within the authors' knowledge, there have been no experimental data reported on the thermal buckling behavior of sandwich panels with truss cores under clamped boundary conditions. By using the folding and brazing method, sandwich panels with pyramidal truss cores are fabricated and used to carry out experimental studies. A load-frame fixture basically following Rakow and Waas's design with slight modifications is applied in the experiment. Consider that the CBT of the fabricated sandwich panel is relatively high (in the region of 300 ~ 500 °C) and that displacement sensors and shadow moiré interferometry may be invalid; the three-dimensional (3-D) digital image correlation (DIC), a noncontact measurement technique, is developed to capture the full-field deformation and the postbuckling behavior of sandwich panels with truss cores tested in high-temperature environment. To verify the precision of the three-dimensional (3-D) digital image correlation (DIC) system, the buckling mode of the thin plate is also tested by the dimensional measurement machine. The experimentally obtained CBT is also compared with that predicted by theoretical and finite-element models.

II. Sandwich Panel Fabrication and Specimen Preparation

Until now, the fabrication of a sandwich panel with a truss core is still in the laboratory-level stage. The folding of a perforated metal sheet provides a simple means to make a lattice truss core [9,10]. In the present work, truss cores with pyramidal configuration were fabricated from a 0.7-mm-thick perforated stainless-steel sheet, obtaining a relative density $\bar{\rho}$ of about 3%. Figure 1 shows the sketch of the punching operation to fold the perforated sheet into pyramidal truss cores, by using a punch-and-die pair of 60 deg angle. To avoid node fracture and enlarge the joint area between truss cores and panels, the punch-and-die pair is designed with a 3 mm terrace to obtain flat areas at nodal regions. Conventional joining methods such as brazing or laser welding can be used to bond the core to solid face sheets to form a sandwich structure. Consider that laser welding may result in flaws in the face sheets; we choose the brazing technique. The solder material is BNi-2, and it can resist a high temperature up to 800°C without failure after bonding. During the brazing period, the sandwich panels are heated up to 1040–1060°C and held for 10–15 min.

A typical fabricated sandwich panel with truss core is shown in Fig. 2. The specimen measures $250 \times 250 \times 8.8$ mm in dimension, and the truss core thickness and face sheet thickness are 7.0 and 0.9 mm, respectively. The unit truss cell is 12×10 mm in length and width.
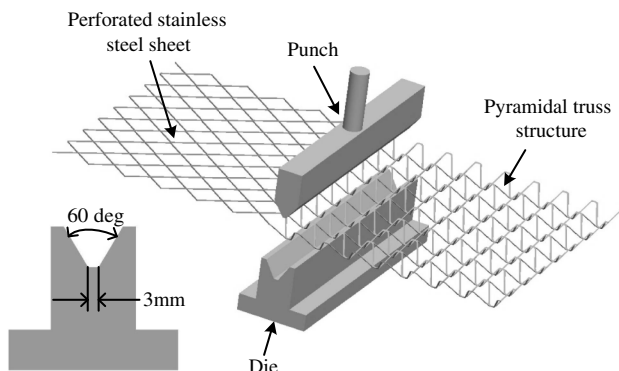

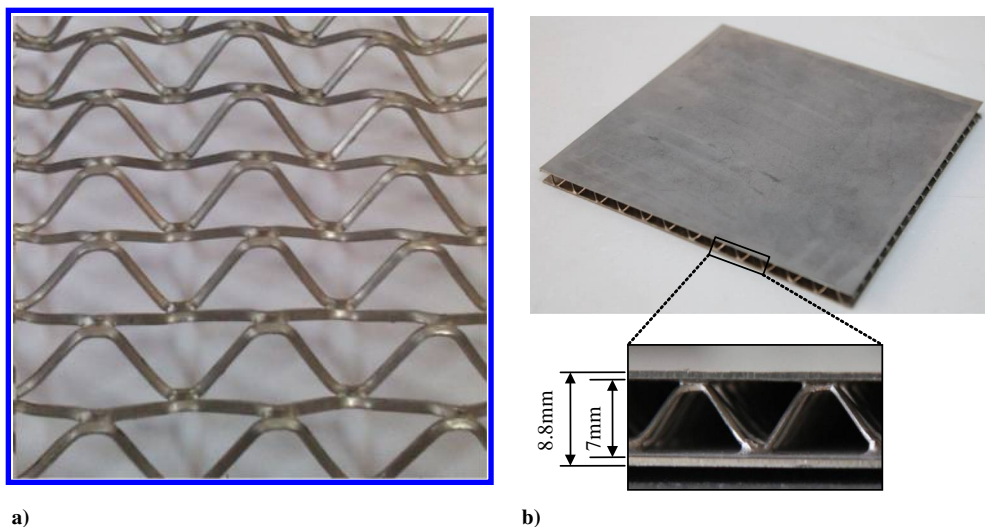Fig. 1 Sketch of the punching operation to manufacture pyramidal truss cores.

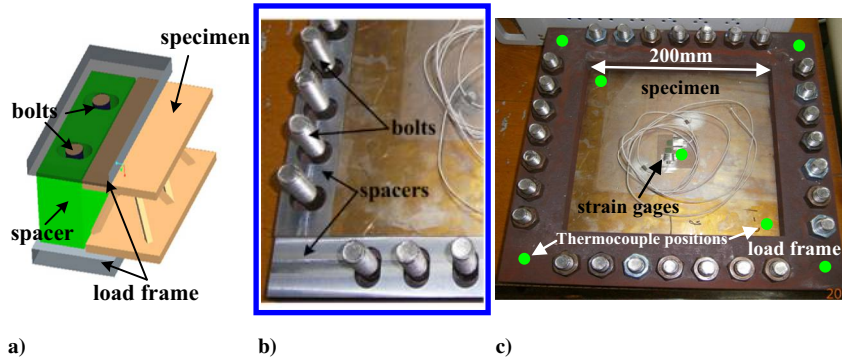Fig. 2 Fabricated sandwich panel: a) folded truss core, and b) a sandwich panel with truss core.

Fig. 3 Load frame and specimen assembly: a) schematic for assembly design, b) during assembly, and c) final assembly.

III.   Experimental Procedure

A.   Experimental Principle and Load-Frame Design

In typical thermomechanical structural experiments, the conflict of thermal and mechanical boundary conditions seems unavoidable; the contacted mechanical load frame acts as a heat sink and compromises the prescribed thermal boundary conditions, and the severity of the thermal loading often degrades the quality of the mechanical boundary conditions [2]. Therefore, it is important to choose an appropriate experimental principle to provide in-plane loading without boundary corruptions in the thermal buckling tests.

We designed a load-frame fixture that basically follows the principle proposed by Rakow and Waas [2]. The central concept is to provide in-plane loads to the specimen by mismatched CTEs between the specimen material and the load frame material, when being heated uniformly and simultaneously. Figure 3 shows the assembly of the sandwich panel and the load frame. The load frame has two identical pieces that were bolted together to provide clamped boundary conditions along borders of the sandwich panel. A slight modification in the present work is that four pieces of spacers were added between the load frame pair against borders of the sandwich panel, to avoid stress concentration and local plastic deformation in the panel. It can be found in the following section on the thermal buckling tests for thin plates carried out by the authors that obvious local yielding is found at the borders when they are directly against the bolts. The load frame leaves a central square test section measuring 200×200 mm. The sandwich panel is made of stainless steel, and the load frame is made of cast iron, which has a lower CTE than the former. The CTE of stainless steel is $18.0 \times 10^{-6}/°C$, whereas the cast iron is $9.0 \times 10^{-6}/°C$ at room temperature. Considering the temperature-dependent CTEs and Young's modulus, the in-plane loading is given by [2]

$$N_T = \int \frac{E(z,T)(\alpha_{\mathrm{frame}}(z,T) - \alpha_{\mathrm{panel}}(z,T))\Delta T(z,T)}{1 - \mu(z,T)}\, \mathrm{d}z \quad (1)$$

where α_{frame} and α_{panel} are the CTEs of the load frame and the sandwich panel, respectively.

B.   Experimental Setup

Figure 4 gives the sketch of experimental setup. Figure 5 shows the actual experimental implement. The load frame and specimen assembly are set in the oven chamber and subjected to a uniform heating cycle, typically at a temperature rise rate of $1.5 °C/\mathrm{min}$. Seven type-K thermocouples, distributed across the top surfaces of both the load frame and the tested sandwich panel, are assembled in the oven to monitor temperature histories of the sample and the load frame. Two of the sandwich panels were instrumented with platinum–8% tungsten strain gauges (type HFP-12-063-SPW, HITEC Products, Inc.) that can withstand a high temperature up to 1038°C. In each specimen, four high-temperature strain gauges were instrumented; two strain gauges orthogonal to each other were attached at the center of the top surface, and the other two were attached at the corresponding position at the bottom surface. The locations of the thermocouples and strain gauges are identified in Fig. 3c. The

observation window, located on the top of the oven, is supplied for cameras to collect images of the specimen during the experiment.

The aim of this experiment is to obtain the critical buckling temperature and the postbuckling behavior of the sandwich panel with truss cores. The CBT is typically determined by strains versus temperature histories, measured from high-temperature strain gauges and thermocouples at the corresponding positions. The postbuckling behavior and full-field deformation can be measured by the modified 3-D–DIC technique, and it also provides CBT information. The two measurement techniques are detailed in the next sections.

C.   Measurement of Critical Buckling Temperature

For the classical thin plate, CBT is defined as the temperature rise at which the CCCC (fully-clamped boundary conditions) plate loses stability, or the bifurcation temperature. The CCCC plate usually buckled in a symmetric mode. For the truss-core sandwich panel studied in the present work, however, there is a competition between overall buckling and local yielding at high temperatures. When the temperature rise approaches 300°C, the total mechanical strain is about 0.5%; therefore, both overall buckling and local yielding are likely to happen. Meanwhile, defects and imperfections during fabrication of the truss-core sandwich panel may result in an asymmetric deformation mode. Therefore, the CBT of the truss-core sandwich panel is defined as the temperature rise at which out-of-plane deformation begins. In general, before CBT, there are only in-plane strains, whereas at the CBT, bending strains begin to occur.

For plates and panels deformed in symmetric mode, the in-plane response and CBT of the sandwich panel can be obtained through strain and temperature histories monitored during the heating period, and the CBT is determined by a Southwell plot analysis of the bifurcation point of the strain gauge pair. The Southwell plot was first given by Southwell [11] for obtaining the critical buckling load of a perfect structure from experimental results on imperfect structures. For the mechanical buckling of a column, the critical buckling load P_{cr} can be obtained by considering
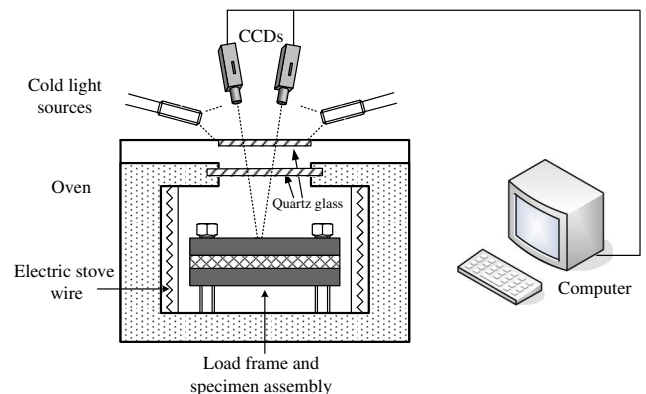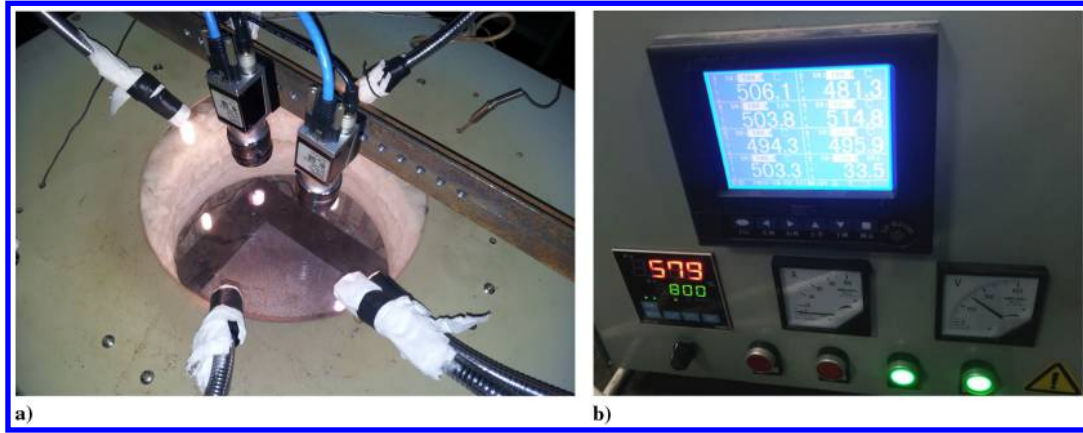

Fig. 4   Sketch of experimental setup.

Fig. 5 Experimental implement: a) 3-D–DIC measurement integrated with the experimental environment, and b) control panel and temperature monitoring.

$$\delta = \frac{P_{\mathrm{cr}}}{P}\delta - \delta_0 \qquad (2)$$

and plotting δ versus δ/P, where δ is the lateral deflection of the midpoint of the column, δ_0 is initial deflection of the imperfect column, and P is the end load. Likewise, the CBT of the sandwich panels is represented by [2]

$$\varepsilon_b = \frac{\Delta T_{\mathrm{cr}}}{\Delta T}\varepsilon_b - w_{0,xx} \qquad (3)$$

where ε_b is the bending strain in the center of the sandwich panel.

For panels deformed in the asymmetric mode, the CBT is monitored by the 3-D–DIC measurement, which is detailed in the following section. The CBT is determined by the temperature rise at which out-of-plane motion can be measured.

D. Measurement of Postbuckling Mode

To capture the postbuckling behavior and full-field deformation history of the sandwich panel, a modified three-dimensional digital image correlation (3-D–DIC) technique that is fit for high-temperature environment is introduced into the thermal buckling experiment. Peters and Ranson [12] first proposed the digital image correlation technique by using the computer-based analysis for planar deformation measurements (two-dimensional DIC). However, this method is limited to planar specimens that experience no out-of-plane motions. Luo et al. [13] solved this problem by using of two digital cameras observing the surface from two different directions (3-D–DIC).

The 3-D–DIC technique is based on both stereo-vision theory and digital image correlation technique. Camera calibration and images matching are two key procedures. In the present experiment, charge-coupled device (CCD) cameras were calibrated by using a certified pasteboard that attached to the silica glass plate panel, and the pasteboard was marked with enough grids to provide high-precision calibration. To provide random gray-value dot patterns that can be observed and recognized by two digital cameras, the top surface of the sandwich panel was sprayed into speckles of suitable size with high-temperature paint. Because the sandwich panel is large and the focal length is small, images captured by the two CCD cameras demonstrate obvious warping and difference, making image matching difficult. Therefore, geometry correction of images must be carried out before the image correlation to obtain reliable deformation reconstruction of the sandwich panel. Figure 6 gives the flowchart of experimental procedure used in the present study, when measuring the postbuckling mode of large-sized panels. In summary, the current experimental procedure includes several steps: 1) sand blasting and speckle painting on the front surface of the sandwich panel, 2) CCD camera calibration with a certified plate, 3) image collection by two cameras, 4) geometry correction of the collected

images, and 5) image correlation and deformation profile reconstruction.

For the gray-value correlation, the normalized covariance correlation function is used in this paper:

$$C(u,v)$$
$$= \frac{\sum_{x'=0}^{m-1}\sum_{y'=0}^{n-1}[I_0(x,y)-\bar{I}_0][I(x'+x,y'+y)-\bar{I}]}{\sqrt{\sum_{x'=0}^{m-1}\sum_{y'=0}^{n-1}[I_0(x,y)-\bar{I}_0]^2}\sqrt{\sum_{x=0}^{m-1}\sum_{y=0}^{n-1}[I(x'+x,y'+y)-\bar{I}]^2}}$$
$$(4)$$

where m and n are the size of the compute template, $I_0(x,y)$ is the gray value of the point (x,y) on the source image, and $I(x',y')$ is the gray value of the point (x',y') on the target image. $\bar{I}_0$ and $\bar{I}$ are the average gray value of compute template on the source and target image, respectively.
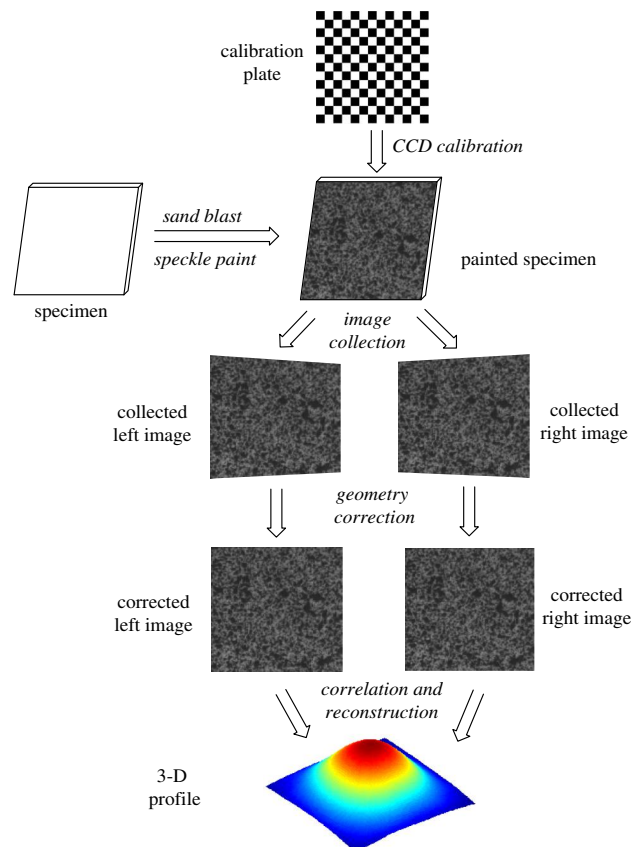

Fig. 6 Flowchart of 3-D deformation profile measurement.

Figure 5 shows the 3-D–DIC equipment integrated with the thermal buckling experimental environment. To make the 3-D–DIC technique fit for the present high-temperature environment, several additional improvements have to be made.

1) First, the oven chamber is dark due to the closed environment, and the darkness hampered image collection and speckle identification. To obtain images that have high correlation factors, the specimen should be tested in the appropriately illuminated environment. Therefore, four cold light sources are employed and placed on top of the observation window during the experiment; see Fig. 5a. Frosted glass plates were attached at the end of the optical fiber to make a uniform light. The as-received sandwich panel was highly reflective under the cold light sources; therefore, the surface was sand blasted before the test to avoid highlights.

2) In addition, speckle images may also be affected by the invisible light shined from the heated electric stove wire. When the heating rate is above 10 °C/min, the invisible light due to thermal radiation intensifies significantly and suppress the illumination light provided by cold light sources. As a result, the image brightness tends to be saturated, and image contrast decreases dramatically, which leads to a serious noncorrelation between collected images. To eliminate this effect, it is necessary to use a filter lens and employ a low temperature rise rate.

3) In the image correlation technique, the specimen surface is usually painted with speckle patterns. In the high-temperature test, the speckle must maintain its color and shape during the heating process. Unexpected changes in the shape may adversely affect the result of the image correlation. The painted speckle must adhere to the surface of the specimen stably and deform simultaneously with the specimen's surface without cracking and peeling off. To solve these problems, a high-temperature paint, which can withstand an up-limit temperature of 800°C, mixed with a special curing agent was used to make the speckle in the present study. Before tests, the speckle was exposed at room temperature for 48 h to ensure that the paint solidifies and adheres firmly on the specimen surface.

IV. Results and Discussions

A. Method Validation with Thin-Plate Buckling Tests

To verify the accuracy of the experimental system and measurement techniques employed in the present study, two 2.7 mm stainless-steel plates and two 4 mm aluminum-alloy plates were tested, subjected to a quasi-statically increasing uniform temperature field.

The verification of CBT can be obtained by comparing experimental results with the classical thin-plate theory predictions, which can be expressed as

$$\Delta T_{cr} = \left(\frac{4\pi^2}{9}\right)\left(\frac{1}{(\alpha_{frame} - \alpha_{panel})(1 + \mu)}\right)\left(\frac{t}{a}\right)^2 \quad (5)$$

where ΔT_{cr} is the CBT, μ is Poisson's ratio, and a and t are the edge length and the thickness of the plate, respectively. Figure 7a shows strain versus temperature histories of the tested thin plate. Strains in the center of top surface and bottom surface of the panel appear consistent at low temperature. Figure 7b shows a Southwell plot of the thin plate to determine the CBT. Table 1 gives the comparison of the CBT measured from experiments and that predicted from thin-plate theory. The data indicate that the difference between theoretical predictions and experimental results is within 12%.

To verify the accuracy of the present 3-D–DIC system, the deformation mode of the buckled thin plate was also tested by the coordinate measurement machine (CMM), a contact measurement technique that has a precision of 2 um. After the thermal buckling experiment, the final buckling mode of the thin plate was measured by the 3-D–DIC technique at room temperature. Then, the deformed specimen was taken out from the oven and tested on the CMM. Figure 8 shows the comparison of deformation modes obtained from 3-D–DIC system and CMM system. The figure indicates that the 3-D–DIC measurement is in a good agreement with the CMM measurement.
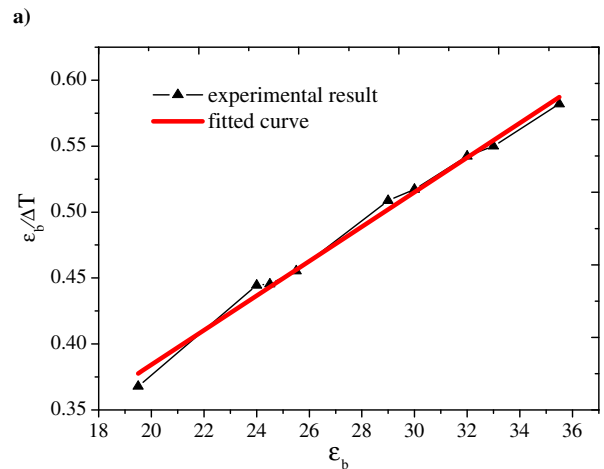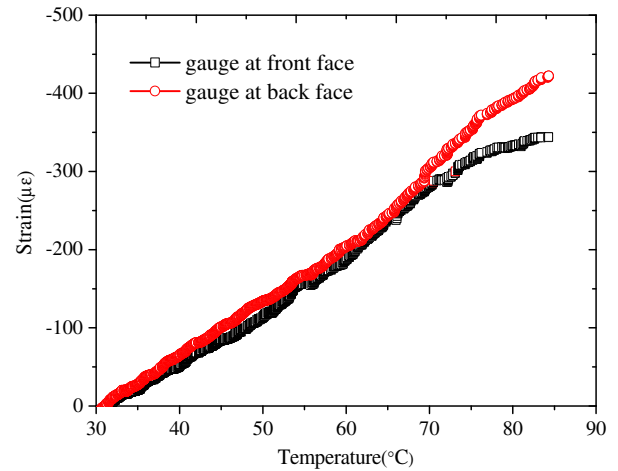

Fig. 7 Thermomechanical response of the thin plate: a) strain vs temperature histories, and b) Southwell plot to determine the CBT.

Figure 9 shows the full-field deformation and buckling history of the thin aluminum plate at different temperature increment. The evolution of tentlike postbuckling mode indicates that the 3-D–DIC captured the thermomechanical response of the plate both temporally and spatially very well. Figure 10 shows the deformation of the central line when the temperature grows. There is no out-of-plane deformation in the thin plate when the temperature is low. When the temperature is greater than the CBT of the thin plate, which is around 95°C, the out-of-plane deformation grows rapidly. Figure 11 shows the out-of-plane deformation of the central point of the plate when the temperature grows, and the experimental result is compared with that of the finite-element model. The onset of buckling agrees well with that of numerical and theoretical predictions, which means that the 3-D–DIC can be used to measure CBT as well. Although the postbuckling out-of-plane deformation obtained from the experiment seems to be lagged, this may due to the imperfect CCCC conditions for thin-plate tests. In the thermal buckling tests for thin plates, the specimen borders are in direct contact against the bolts, and local yielding is found at the discrete positions; see enlarged border image of the tested thin plate in Fig. 11. The in-plane plastic deformation may consume part of the out-of-plane deformation.

Table 1   Critical buckling temperature of the thin plate

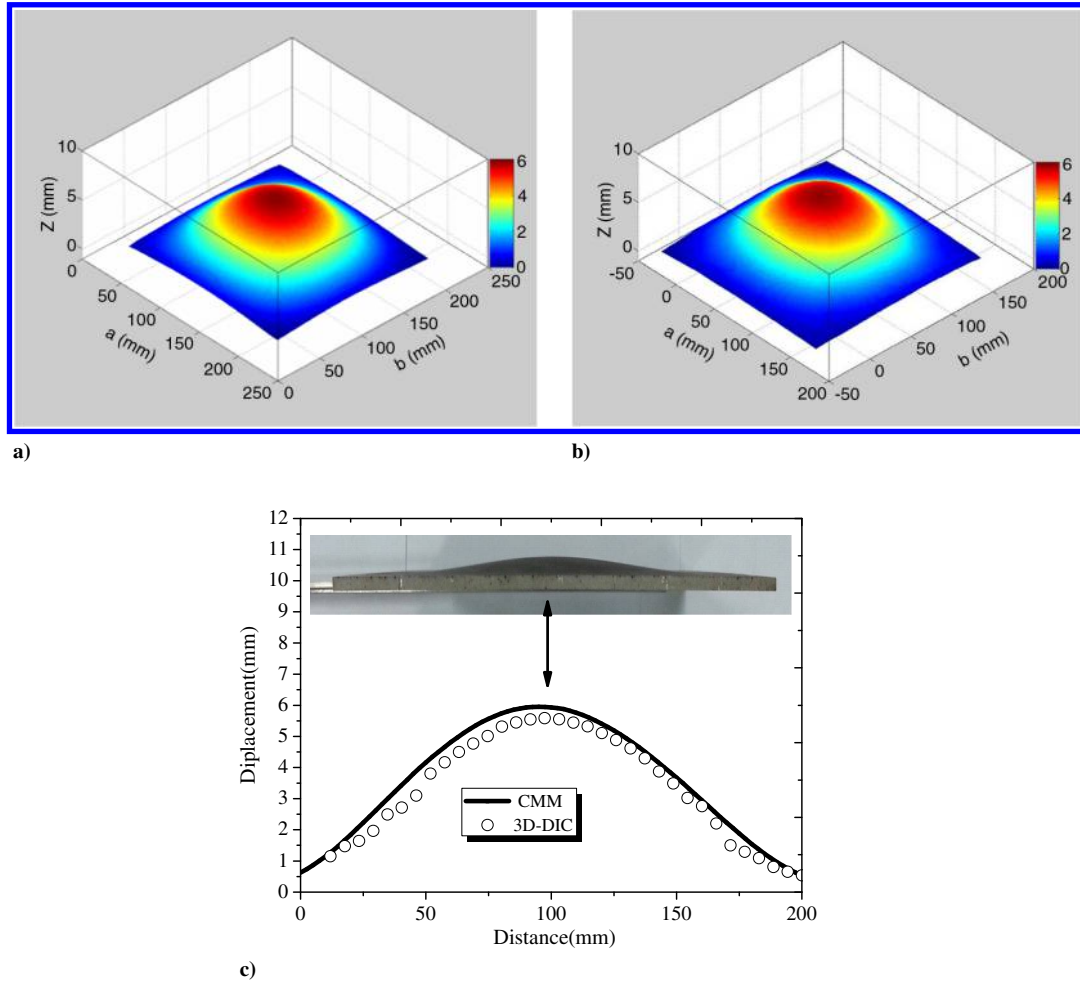| Theoretical and experimental results	ΔT_{cr}, °C	Difference, %
Theoretical predication	68	— —
Experimental result (test 1)	76	11.7
Experimental result (test 2)	64	6.0

a)

b)

c)

Fig. 8   Comparison of 3-D–DIC and CMM: a) CMM measurement, b) 3-D–DIC measurement, and c) comparison deformations along the centerline.

B.   Critical Buckling Temperature of the Sandwich Panel

In the thin-plate tests, the specimen directly contacted the fixture bolts, and local yielding is found. In the sandwich panel tests, spacers were used to prevent direct contact between the specimen and the bolts, as shown in Fig. 3. Four specimens of the sandwich panel with truss core were tested in the present study; two of the specimens were instrumented with high-temperature strain gauges to obtain the in-plane response and the CBT. Specimens were also monitored by 3-D–DIC, measuring CBTs as well as the full-field out-of-plane deformation history as the panel deformed into the postbuckling regime.

Figure 12a shows locations of thermocouples and temperature histories during heating. Mechanical strain versus temperature histories are shown in Fig. 12b. Strains in the center of top surface and bottom surface of the panel appear consistent at low temperature. The Southwell plot in Fig. 12c indicates that the experimentally obtained CBT is 347°C.

For sandwich panels under CCCC conditions (fully clamped), the CBT cannot be analytically solved as that under simply supported conditions because the governing equations for the deformation mode is complicated due to the complex boundary conditions. Thus, the CBT is solved through the method of double Fourier expansions to the virtual deformation mode by using the Ressiner model. The equilibrium equation of the sandwich panel can be expressed as

$$D\left(\frac{\partial^2 \phi_x}{\partial x^2} + \frac{1-\mu}{2}\frac{\partial^2 \phi_x}{\partial y^2} + \frac{1+\mu}{2}\frac{\partial^2 \phi_y}{\partial x \partial y}\right) + C\left(\frac{\partial w}{\partial x} - \phi_x\right) = 0 \quad (6a)$$

$$D\left(\frac{\partial^2 \phi_y}{\partial y^2} + \frac{1-\mu}{2}\frac{\partial^2 \phi_y}{\partial x^2} + \frac{1+\mu}{2}\frac{\partial^2 \phi_x}{\partial x \partial y}\right) + C\left(\frac{\partial w}{\partial y} - \phi_y\right) = 0 \quad (6b)$$

$$D\left(\frac{\partial^2 w}{\partial x^2} + \frac{\partial^2 w}{\partial y^2} - \frac{\partial \phi_x}{\partial x} - \frac{\partial \phi_y}{\partial y}\right) + N\nabla^2 w = 0 \quad (6c)$$

The shear stiffness of the sandwich panel is derived by considering the deformation of one unit cell and assuming that the truss is straight under the shear force. When applying a shear force F on one side of the panel, the displacement can be expressed as

$$\Delta_{\text{pyramid}} = \frac{Fh_c}{2ES\sin^3\omega} \quad (7a)$$

The shearing strain can be derived:

$$\varepsilon_{\text{pyramid}} = \frac{\Delta_{\text{pyramid}}}{h_c} = \frac{F}{2ES\sin^3\omega} \quad (7b)$$

Then, the shear modulus can be obtained:

$$C = G_{\text{pyramid}}h_c = \frac{ES\sin^3\omega}{h_c} \quad (7c)$$

Consider the CCCC boundary condition; the following virtual displacement mode is assumed:

$$w = \sum_{m=1}^{\infty}\sum_{n=1}^{\infty} A_{mn}\sin\alpha_m x\sin\beta_n y \quad (8a)$$

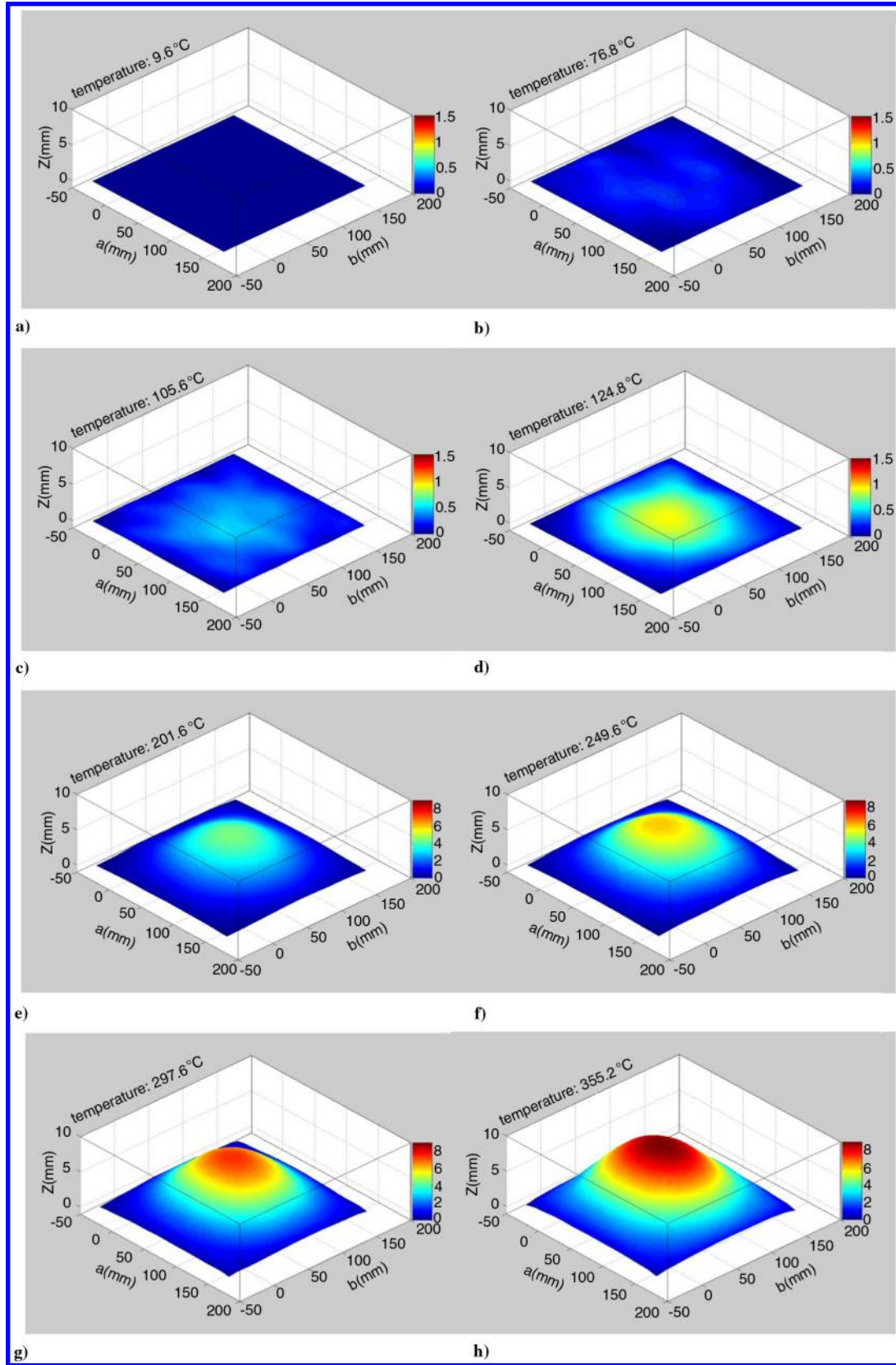$$\phi_x = \sum_{m=1}^{\infty}\sum_{n=1}^{\infty} B_{mn}\sin\alpha_m x\sin\beta_n y \quad (8b)$$

Fig. 9 Full-field deformation and buckling history of the thin plate, with a temperature rise ΔT of a) 9.6°C, b) 76.8°C, c) 105.6°C, d) 124.8°C, e) 201.6°C, f) 249.6°C, g) 297.6°C, and h) 355.2°C.

$$\phi_y = \sum_{m=1}^{\infty} \sum_{n=1}^{\infty} C_{mn} \sin \alpha_m x \sin \beta_n y \qquad (8c)$$

Then the characteristic equation can be written as

$$\sum_{m=1}^{\infty} \sum_{n=1}^{\infty} \left(\frac{\mu - 1}{2} D\beta_n^2 - D\alpha_m^2 - C \right) B_{mn} + \sum_{r=1}^{\infty} h_{rm} CA_{rn}\gamma_r$$

$$+ \sum_{r=1}^{\infty} \sum_{s=1}^{\infty} h_{rm} h_{sn} \frac{1 + \mu}{2} DC_{rs}\gamma_r\psi_s = 0 \qquad (9a)$$
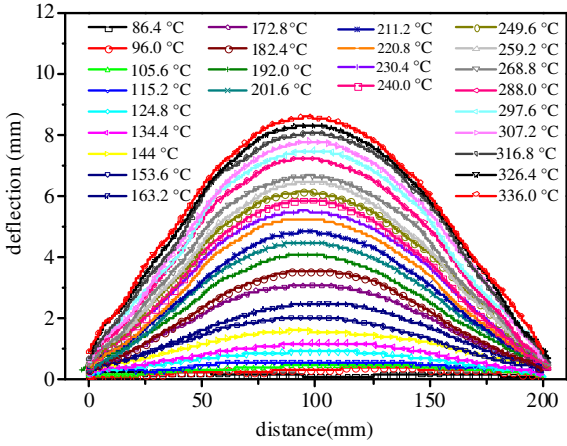
Fig. 10 Deformation history along the centerline of the thin plate at different temperature rise.
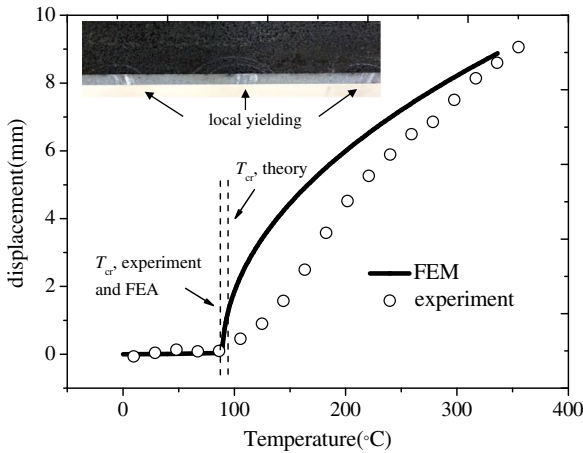

Fig. 11 Comparison of out-of-plane deformation histories at the center point between experimental and numerical results.

$$\sum_{m=1}^{\infty}\sum_{n=1}^{\infty}\left\{\left(\frac{\mu-1}{2}D\alpha_m^2 - D\beta_n^2 - C\right)C_{mn} + \sum_{s=1}^{\infty}h_{sn}CA_{ms}\psi_s\right.$$
$$\left. + \sum_{r=1}^{\infty}\sum_{s=1}^{\infty}h_{rm}h_{sn}\frac{1+\mu}{2}DB_{rs}\gamma_r\psi_s\right\} = 0 \qquad (9b)$$

$$\sum_{m=1}^{\infty}\sum_{n=1}^{\infty}\left\{-[C(A_{mn}\alpha_m^2 + A_{mn}\beta_n^2)] - \sum_{s=1}^{\infty}h_{sn}CC_{ms}\psi_s\right.$$
$$\left. - \sum_{r=1}^{\infty}h_{rm}CB_{rn}\gamma_r\right\} - N\sum_{m=1}^{\infty}\sum_{n=1}^{\infty}[(A_{mn}\alpha_m^2 + A_{mn}\beta_n^2)] = 0 \qquad (9c)$$

This equation should be solved numerically due to the large numbers of the Fourier expansions. A computer program is developed to solve Eq. (9) by calling the subroutine GVCRG of IMSL, which is used to solve eigenvalue problems [14]. The CBT solved by the theoretical analysis is 499°C. The discrepancy of theoretically predicted and experimentally obtained CBT may attribute to defects of the panel and the truss core during fabrication. Defects, including bonding flaws at brazing areas and truss distortion and bending, affect the buckling performance of the sandwich panel significantly. Approximately 5% of the total nodes may break under the compression of the press brake, and these defects reduce the shear stiffness of the sandwich panel. Likewise, in the theoretical analysis, the truss is supposed to be straight, and the core is in the stretching-dominated configuration. However, the distortion and bending of the truss turn
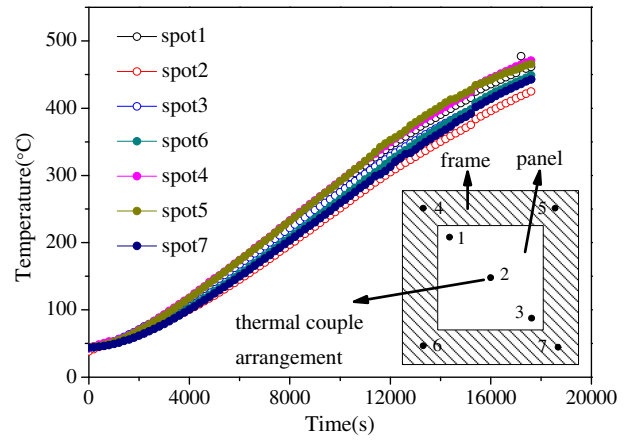
a)
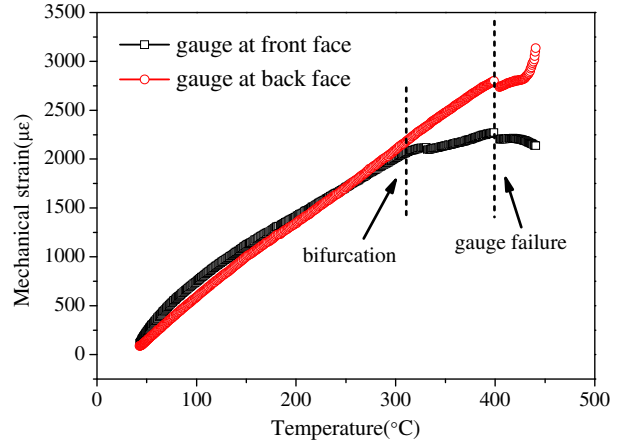
b)
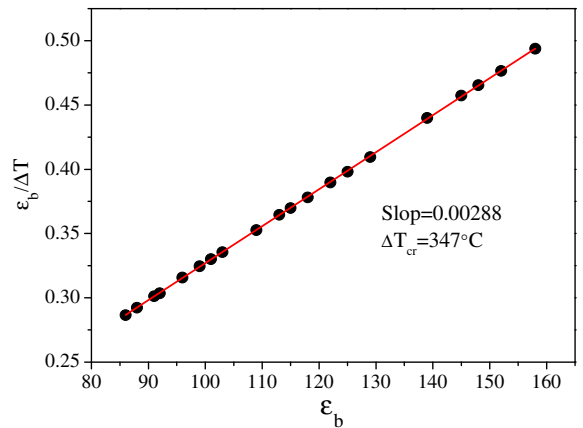
c)

Fig. 12 Thermomechanical response of the sandwich panel: a) temperature histories and locations of thermocouples, b) mechanical strains vs temperature, and c) Southwell plot to determine the CBT of the sandwich panel.

the core into bending-dominated materials. For cellular materials, the modulus can be written into [15–18]

$$E^* = \alpha E_s(\bar{\rho})^n \qquad (10)$$

where E_s is the Young's modulus of the parent material, $\bar{\rho}$ is the relative density of the cellular material, α and n are the coefficient and the exponent, respectively. For bending-dominated materials such as metal foams, the modulus scales as $\bar{\rho}^2$, whereas for stretching-dominated materials such as truss cores, the modulus scales as $\bar{\rho}$. It is worth noting that many experimentally measured moduli for lattice trusses are well below the predicted

values [9,10]. Therefore, the actual stiffness of the fabricated sandwich panel is dramatically lower than that applied in the theoretical model in Eq. (7). A correction factor is introduced to measure the effect of defects on the stiffness of the sandwich panel with truss cores:

$$\eta = \frac{C_s}{C} \qquad (11)$$

where C_s and C are the actual shear stiffness of the sandwich panel and that is used in the theoretical analysis, respectively. The correction factor is around 0.61 in the present study.

C. Postbuckling Behavior of the Sandwich Panel

Figure 13 is the full-field deformation history of the sandwich panel with truss core, measured from 3-D–DIC. At a temperature

of about 297°C, the panel begin to buckle. The initial out-of-plane deformation is not at the center of the panel, probably due to the defects. Therefore, the whole postbuckling deformation process is not symmetric. Figure 14 shows the three-dimensional reconstruction of the final deformation mode of another sandwich panel. According to the images captured by 3-D–DIC and the visual observation of the tested sandwich panel specimen, local yielding in addition to overall buckling is the primary failure mode. The local yielding may be induced by fabrication defects in several ways, which have been summarized in the previous section.

V. Conclusions

With the aid of the specifically designed load frame and measurement techniques, experimental investigation of the thermal buckling behavior of sandwich panels with pyramidal truss cores is carried out. The study provides the firsthand measurement data for the
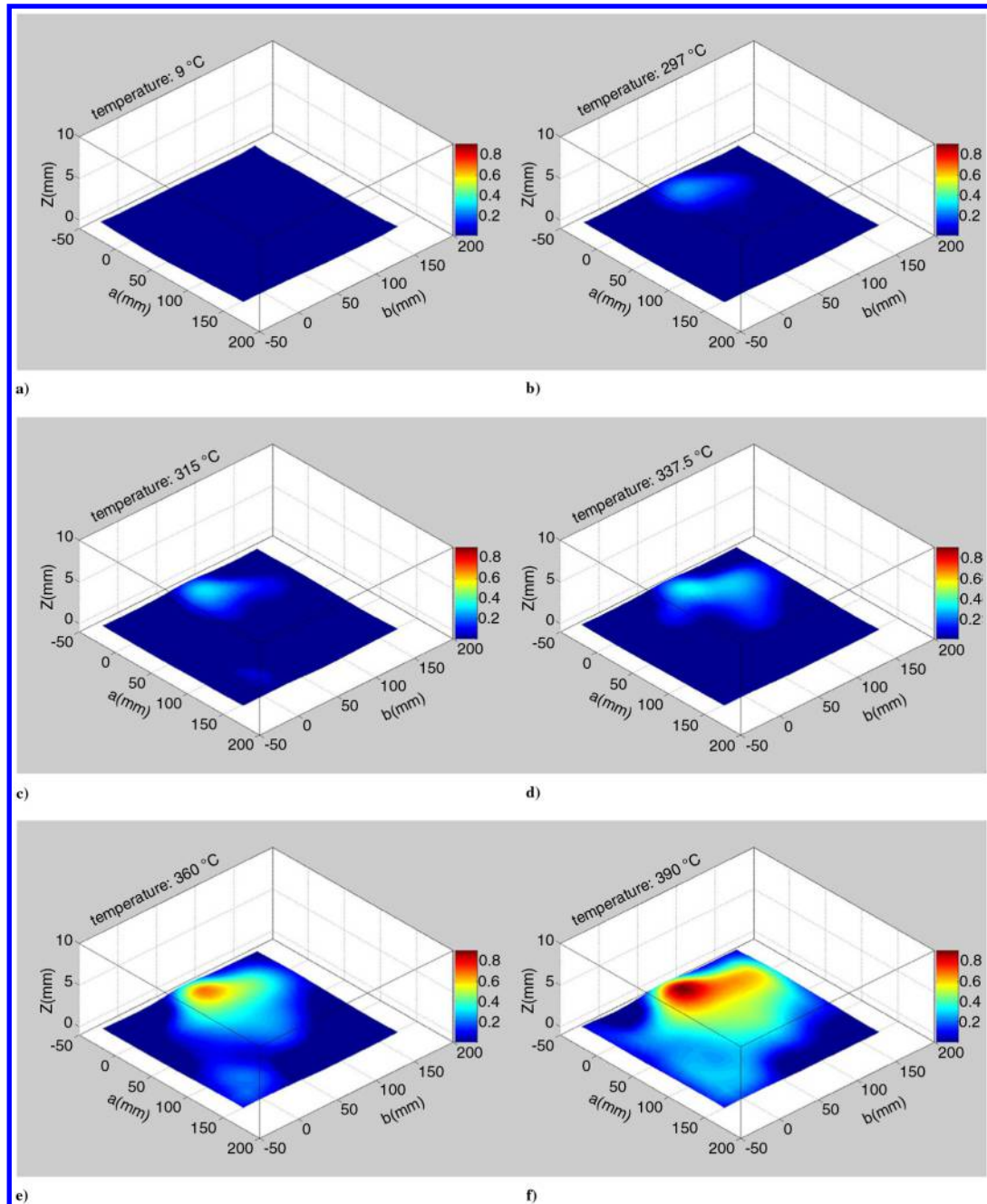

Fig. 13   Full-field deformation history of the sandwich panel, with a temperature rise ΔT of a) 9°C, b) 297°C, c) 315°C, d) 337.5°C, e) 360°C, and f) 390°C.
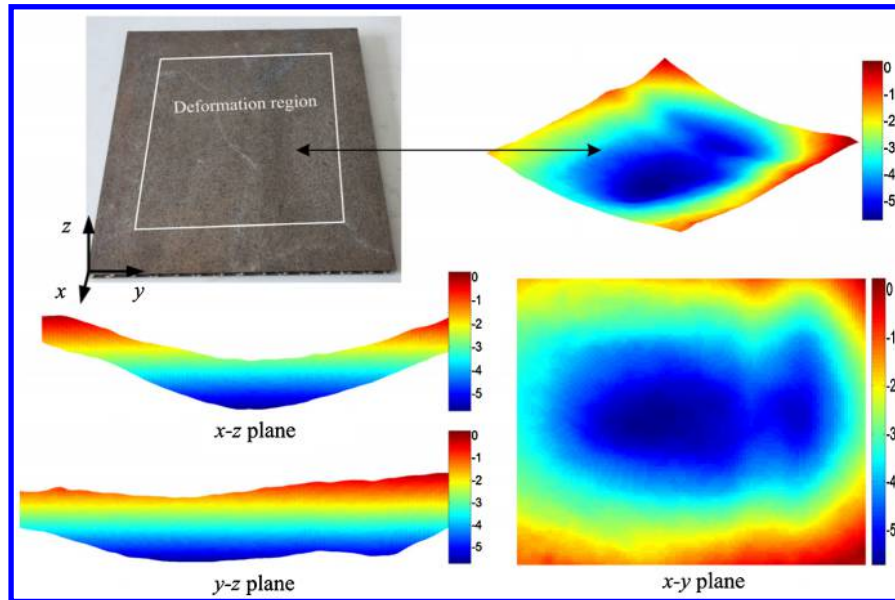
Fig. 14   Full-field deformation of the sandwich panel, 3-D–DIC result.

thermal buckling behavior of sandwich panels with truss cores. The CBT of the sandwich panel is determined from strain–temperature histories at the center of face sheets by using the Southwell method and by the noncontact 3-D–DIC technique. According to experiments, the CBT of the sandwich panel is around 297–347°C, which is lower than that predicted from the analytical model. This discrepancy may be attributed to defects and imperfections of the truss core and sandwich panel during fabrication. Defects of the truss core make the Young's modulus and shear stiffness dramatically lower than that assumed in the theoretical model. The noncontact 3-D–DIC technique is adopted to measure the full-field deformation history of the sandwich panels in the postbuckling regime. The precision of 3-D–DIC is verified by CMM measurement. Again, because of defects, the postbuckling mode of the sandwich is not uniform. Typically, local yielding together with overall buckling is found in the tested specimen.

Acknowledgments

References

[1] Singer, J., Arbocz, J., and Weller, T., *Buckling Experiments: Experimental Methods in Buckling of Thin-Walled Structures*, Wiley, Hoboken, NJ, 2002, pp. 1550–1555.

[2] Rakow, J. F., and Waas, A. M., "Thermal Buckling of Metal Foam Sandwich Panels for Convective Thermal Protection Systems," *Journal of Spacecraft and Rockets*, Vol. 42, No. 5, 2005, pp. 832–844.
doi:10.2514/1.9741

[3] Rakow, J. F., and Waas, A. M., "Response of Actively Cooled Metal Foam Sandwich Panels Exposed to Thermal Loading," *AIAA Journal*, Vol. 45, No. 2, 2007, pp. 329–336.
doi:10.2514/1.24813

[4] Gossard, M. L., Seide, P., and Roberts, W. M., "Thermal Buckling of Plates," NACA TN-2771, 1952.

[5] Murphy, K. D., and Ferreira, D., "Thermal Buckling of Rectangular Plates," *International Journal of Solids and Structures*, Vol. 38, Nos. 22–23, 2001, pp. 3979–3994.
doi:10.1016/S0020-7683(00)00240-7

[6] Thornton, E. A., Coyle, M. F., and McLeod, R. N., "Experimental Study of Plate Buckling Induced by Spatial Temperature Gradients," *Journal of Thermal Stresses*, Vol. 17, No. 2, 1994, pp. 191–212.
doi:10.1080/01495739408946255

[7] Blosser, M., "Boundary Conditions for Aerospace Thermal–Structural Tests," *Progress in Astronautics and Aeronautics*, Vol. 168, 1995, pp. 119–144.

[8] Richards, W. L., and Thompson, R. C., "Titanium Honeycomb Panel Testing," NASA TM-4768, 1996.

[9] Wadley, H. N., Fleck, N. A., and Evans, A. G., "Fabrication and Structural Performance of Periodic Cellular Metal Sandwich Structures," *Composites Science and Technology*, Vol. 63, No. 16, 2003, pp. 2331–2343.
doi:10.1016/S0266-3538(03)00266-5

[10] Wadley, H. N., "Multifunctional Periodic Cellular Metals," *Philosophical Transactions of the Royal Society A*, Vol. 364, No. 1838, 2006, pp. 31–68.
doi:10.1098/rsta.2005.1697

[11] Southwell, R. V., "On the Analysis of Experimental Observations in Problems of Elastic Stability," *Proceedings of the Royal Society of London Series A*, Vol. 135, 1932, pp. 601–616.
doi:10.1098/rspa.1932.0055

[12] Peters, W., and Ranson, W., "Digital Imaging Techniques in Experimental Stress Analysis," *Optical Engineering*, Vol. 21, No. 3, 1982, pp. 427–431.

[13] Luo, P., Chao, Y., Sutton, M., and Peters, W., III, "Accurate Measurement of Three-Dimensional Deformations in Deformable and Rigid Bodies Using Computer Vision," *Experimental Mechanics*, Vol. 33, No. 2, 1993, pp. 123–132.
doi:10.1007/BF02322488

[14] Yuan, W., Wang, X., Song, H. W., and Huang, C. G., "A Theoretical Analysis on the Thermal Buckling Behavior of Fully-Clamped Sandwich Panels with Truss Cores" *Journal of Thermal Stresses*, Vol. 37, No. 12, 2014, pp. 1433–1448.

[15] Deshpande, V., Ashby, M., and Fleck, N., "Foam Topology: Bending Versus Stretching Dominated Architectures," *Acta Materialia*, Vol. 49, No. 6, 2001, pp. 1035–1040.
doi:10.1016/S1359-6454(00)00379-7

[16] Deshpande, V., Fleck, N., and Ashby, M., "Effective Properties of the Octet-Truss Lattice Material," *Journal of the Mechanics and Physics of Solids*, Vol. 49, No. 8, 2001, pp. 1747–1769.
doi:10.1016/S0022-5096(01)00010-2

[17] Evans, A. G., Hutchinson, J. W., and Ashby, M. F., "Multifunctionality of Cellular Metal Systems," *Progress in Materials Science*, Vol. 43, No. 3, 1998, pp. 171–221.
doi:10.1016/S0079-6425(98)00004-8

[18] Gibson, L. J., and Ashby, M. F., *Cellular Solids: Structures and Properties*, Cambridge Univ. Press, Cambridge, England, U.K., 1997, pp. 183–217.

S. Pellegrino
Associate Editor